Dzyaloshinskii-Moriya interactions and adiabatic magnetization dynamics in molecular magnets

H. De Raedt,[1,*] S. Miyashita,[2,†] K. Michielsen,[1,‡] and M. Machida[2,§]

[1]*Department of Applied Physics, Materials Science Centre, University of Groningen, Nijenborgh 4,*
NL-9747 AG Groningen, The Netherlands
[2]*Department of Applied Physics, Graduate School of Engineering, University of Tokyo, Bunkyo-ku, Tokyo 113-8656, Japan*

A microscopic model of the molecular magnet V_{15} is used to study mechanisms for the adiabatic change of the magnetization in time-dependent magnetic fields. The effects of the Dzyaloshinskii-Moriya interaction, the most plausible source for the energy-level repulsions that lead to adiabatic changes of the magnetization, are studied in detail. We find that the energy-level repulsions that result from this interaction exhibit a strong dependence on the direction of the applied field. We also discuss the role of magnetic anisotropy in the molecule Mn_{12}-acetate.

I. INTRODUCTION

Recently, magnetic molecules such as Mn_{12} or V_{15} have attracted a lot of interest. These nanomagnets are often used to study explicit real-time quantum dynamics, e.g., tunneling of the magnetization and quantum (de)coherence.[1–22] As a result of the very weak intermolecular interactions, experiments can directly probe the magnetization dynamics of the individual molecules. In particular, the adiabatic change of the magnetization at low temperature is governed by the discrete energy-level structure.[23–27]

The adiabatic change of the magnetization requires some interactions that yield energy-level repulsions, i.e., interactions that do not commute with the magnetization. The Dzyaloshinskii-Moriya (DM) interaction is the most likely candidate for such an interaction.[11,28,29] In the case of anisotropic high-spin molecules such as Mn_{12} and Fe_8, simplified anisotropic single-spin models for a specific spin multiplet can approximately reproduce the gaps of the level repulsions. However, the case of V_{15} is more complicated because V_{15} has half-odd-integer spin and the time-reversal symmetry enforces at least a twofold degeneracy of the energy levels at zero field.

The possibility that the DM interaction might be the main mechanism for the adiabatic change for the magnetization in V_{15} has been explored in earlier work[29,30] but the dependence of the energy-level scheme on the direction of the magnetic field was not considered. In this paper we further elaborate on this issue and demonstrate that the effect of the DM interaction on the magnetization dynamics strongly depends on the direction of the applied magnetic field. This directional dependence has not been observed in experiments on V_{15}. Therefore the DM interaction generally does not explain why the magnetization changes as the magnetic field is swept.

It has been pointed out that the DM interaction is accompanied by a higher-order correction term that restores the SU(2) symmetry.[31–34] In this paper, we focus on the effects of the DM interaction and leave the inclusion of the higher-order term for future study. As another source of level repulsion, we might consider the hyperfine interaction with the nuclear spin. The effects of the hyperfine interaction have already been discussed in Ref. 52.

As the DM interaction has a vector character and is anisotropic, the dynamics of the magnetization is expected to depend on the direction of the magnetic field. First we study the characteristic properties of the DM interaction for a simplified model of V_{15}, namely, three spins on a triangle. Then we confirm the properties found in the three-spin model by full diagonalization of the 15-spin model of V_{15}. In order to bridge the energy scales involved (e.g., from 800 K, a typical energy scale for the interaction between individual magnetic ions, to about 10^{-2} K, a typical energy scale for energy-level splittings), the calculation of the energy levels of the many-spin Hamiltonian has to be very accurate. We have tested various standard algorithms to compute the low-lying states. For systems that are too large to be solved by full exact diagonalization (such as the 15-spin V_{15} model), we use the Lanczos method with full orthogonalization (LFO), a Chebyshev polynomial projector (CPP) method, and a power method with additional subspace diagonalization. These algorithms can solve the rather large eigenvalue problems with sufficient accuracy. The consistency of the data obtained by different methods gives extra confidence in the numerical results.

The magnetic properties of molecules such as Mn_{12} are often studied by considering a simplified model for the magnetic energy levels for a specific spin multiplet, e.g., $S=10$. However, for these and other, similar, magnetic molecules that consist of several magnetic moments [in the case of Mn_{12}, eight Mn^{3+} ($S=2$) and four Mn^{4+} ($S=3/2$)], the reduction of the many-body Hamiltonian to an effective Hamiltonian for a specific spin multiplet is nontrivial. Magnetic anisotropy, a result of the geometrical arrangement of the magnetic ions within a molecule of low symmetry, mixes states of different total spin and enforces a treatment of the full Hilbert space of the system. For Mn_{12}, the dominant contribution to the magnetic mixing due to spin-orbit interactions is also given by the DM interaction.[35,36] In principle, this type of interaction can change energy-level crossings into energy-level repulsions. The presence of the latter is essential to explain the adiabatic changes of the magnetization at the resonant fields.[23–27] Thus, a minimal magnetic model Hamiltonian should contain (strong) Heisenberg inter-

70 064401-1

actions, DM interactions, and a coupling to the applied magnetic field.[11,28–30,37–42] Experiments on Mn_{12} suggest that the energy gaps related to the transition from a state with magnetization $M \approx -10$ to a state with magnetization $M < 4$ are of the order of 10^{-9} K.[43] Such gaps are too small to detect with standard precision (13–14 digits) calculations, and therefore in this paper we present only the global energy-level diagram obtained from microscopic model calculations.

The paper is organized as follows. In Sec. II we analyze a reduced three-spin model with C_3 symmetry for the V_{15} molecule. Results for the energy-level schemes for a 15-spin model of the V_{15} are presented in Sec. III. In Sec. IV we discuss the effects of anisotropic terms and the cases with less symmetry. In Sec. V, we report results for Mn_{12}. In Sec. VI we give our conclusions. In Appendixes A and B, we briefly discuss some analytical solutions and the numerical algorithms that we use to compute the energy levels, respectively.

II. TRIANGLE MODEL WITH C_3 SYMMETRY

The V_{15} molecule has C_3 symmetry but is not invariant for mirror reflection about the triangle plane. Therefore we take as a simplified model for the V_{15} molecule, a system of three spins on a triangle with C_3 symmetry only. We choose the z axis to lie along the axis of C_3 symmetry. The Hamiltonian is given by

$$\mathcal{H} = -\sum_{i=1}^{3} J_{i,i+1} \mathbf{S}_i \cdot \mathbf{S}_{i+1} + \sum_{\langle i,j \rangle} \mathbf{D}_{i,j} \cdot [\mathbf{S}_i \times \mathbf{S}_j] - \mathbf{h} \cdot \left(\sum_i \mathbf{S}_i \right),$$
(1)

where $J_{1,2}=J_{2,3}=J_{3,1} \equiv J$ denotes the exchange interaction and $\mathbf{h}$ represents the applied magnetic field. In general we can choose any direction of the DM vector $\mathbf{D}_{i,j}$ unless there is some additional symmetry. In the present case, because of the C_3 symmetry, the z component of the DM vectors must all be equal, i.e.,

$$D_{1,2}^z = D_{2,3}^z = D_{3,1}^z \equiv D_z.$$
(2)

If the system has mirror reflection symmetry about the triangle plane then $D_z = 0$. The x and y components of the DM vector, $D_{i,j}^x$ and $D_{i,j}^y$, must obey the relation

$$\begin{pmatrix} D_{2,3}^x \\ D_{2,3}^y \end{pmatrix} = \begin{pmatrix} -\dfrac{1}{2} & \dfrac{\sqrt{3}}{2} \\ -\dfrac{\sqrt{3}}{2} & -\dfrac{1}{2} \end{pmatrix} \begin{pmatrix} D_x \\ D_y \end{pmatrix},$$

$$\begin{pmatrix} D_{3,1}^x \\ D_{3,1}^y \end{pmatrix} = \begin{pmatrix} -\dfrac{1}{2} & -\dfrac{\sqrt{3}}{2} \\ \dfrac{\sqrt{3}}{2} & -\dfrac{1}{2} \end{pmatrix} \begin{pmatrix} D_x \\ D_y \end{pmatrix},$$
(3)

where $D_x \equiv D_{1,2}^x$ and $D_y \equiv D_{1,2}^y$.

In Appendix A we give the analytic expressions for the eigenvalues and eigenvectors of model (1) in the case that
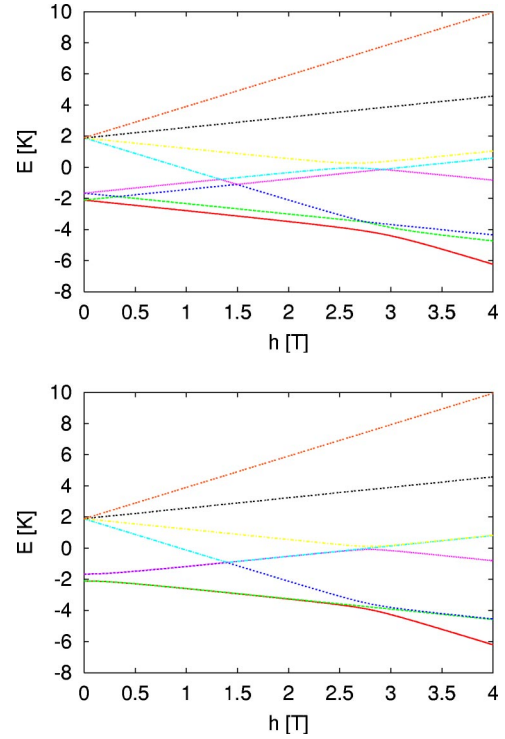

FIG. 1. (Color online) Energy levels of Hamiltonian (1) for $J = -2.5$ K, $D_x = D_y = D_z = 0.25$ K. At each value of h the slope of each level gives the corresponding value of the projection of the total magnetization on the magnetic field axis. Top: Applied magnetic field $\mathbf{h}$ parallel to the z axis. Bottom: Applied magnetic field $\mathbf{h}$ along the x axis.

the applied field is parallel to the z axis and the conditions (2) and (3) hold. Then the Hamiltonian (1) is block diagonal, the matrix containing four blocks of 2×2 matrices. The (eight-dimensional) Hilbert space separates into four two-dimensional spaces:

$$\{|3/2, 3/2\rangle, |a\rangle\}, \quad \{|3/2, 1/2\rangle, |\bar{a}\rangle\},$$

$$\{|3/2, 1/2\rangle, |\bar{b}\rangle\}, \quad \{|3/2, 3/2\rangle, |b\rangle\},$$
(4)

where the state $|S, M\rangle$ denotes an eigenstate of the Heisenberg model with total spin S and magnetization M. The expressions for the orthonormal states $|a\rangle$ and $|b\rangle$ are given in Appendix A. The state $|\bar{a}\rangle$ ($|\bar{b}\rangle$) denotes the state $|a\rangle$ ($|b\rangle$) with all spins reversed. From Eq. (4) it follows that there is no mixing among the four levels with $S = \pm 1/2$, and therefore they simply cross each other. From the analytical solution it is also easy to see that there are no energy-level repulsions at $h=0$. Furthermore, one can show analytically that it is impossible to change the magnetization from $-3/2$ to $+3/2$ by (adiabatically) reversing the external field along the z axis.[28]

In the top panel of Fig. 1 we show the energy levels as a function of the strength h of the applied magnetic field for the case $D_x = D_y = D_z$. The field is aligned along the z axis. It is evident that there is no level mixing at $h=0$. It is important to note that the small energy difference between the first
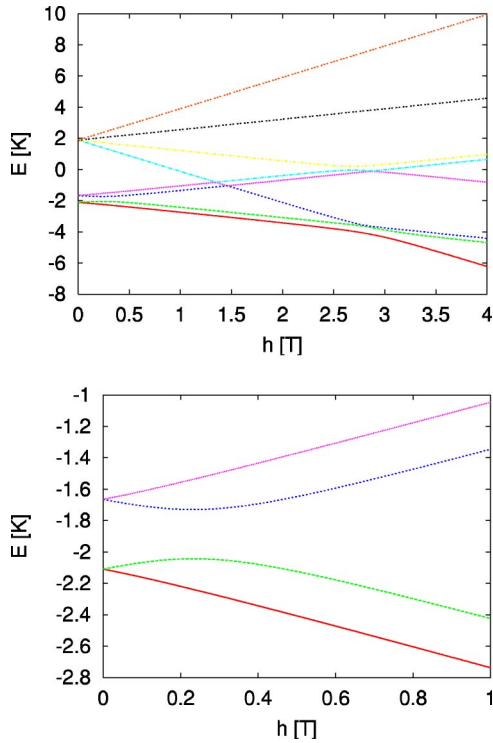
FIG. 2. (Color online) Top: Energy levels of Hamiltonian (1) for $J=-2.5$ K, $D_x=D_y=D_z=0.25$ K, and the applied magnetic field **h** $=h(1,0,1)/\sqrt{2}$ tilted by 45° with respect to the z axis. Bottom: Detailed view of the h dependence of the four lowest energy levels. At each value of h the slope of each level gives the corresponding value of the projection of the total magnetization on the magnetic field axis.

excited state and the degenerate ground states at $h=0$ is not the minimum energy difference of the avoided level crossing (near $h=0$). Therefore, at $h=0$ there is no adiabatic change of the magnetization. On the other hand, if we apply the magnetization along the x direction (i.e., perpendicular to the symmetry axis of the triangle), then two of the states become degenerate. We find two nearly degenerate avoided level crossings, as shown in the bottom panel of Fig. 1. As an intermediate case, in Fig. 2 we show the energy-level diagram for the case that the magnetic field is tilted by 45° with respect to the z axis [$\mathbf{h}=h(1,0,1)/\sqrt{2}$]. Then, there is a simple crossing at zero field and an avoided level crossing between the levels of $M=\pm 1/2$ at a finite magnetic field. Indeed, a closer look at the level diagram (see the bottom panel in Fig. 2) reveals that the minimum energy difference between the two pairs of levels does not occur at zero field but at $h\approx 0.35$ T. This implies that the Landau-Zener-Stückelberg transition from the $|1/2,-1/2\rangle$ to the $|1/2,1/2\rangle$ level does not take place at $h=0$ but at $h\approx 0.35$ T. In conclusion, the position and the energy splitting of the avoided level crossing that is responsible for the adiabatic change depend on the direction of the field.

The numerical results discussed above have been obtained for $D_x=D_y=D_z$. In Ref. 22 the DM vector is taken parallel to the y axis at all the bonds and the field is applied along the z axis. For the present model, this case corresponds to the case with only D_z ($D_x=D_y=0$) and a field applied in the x direc-
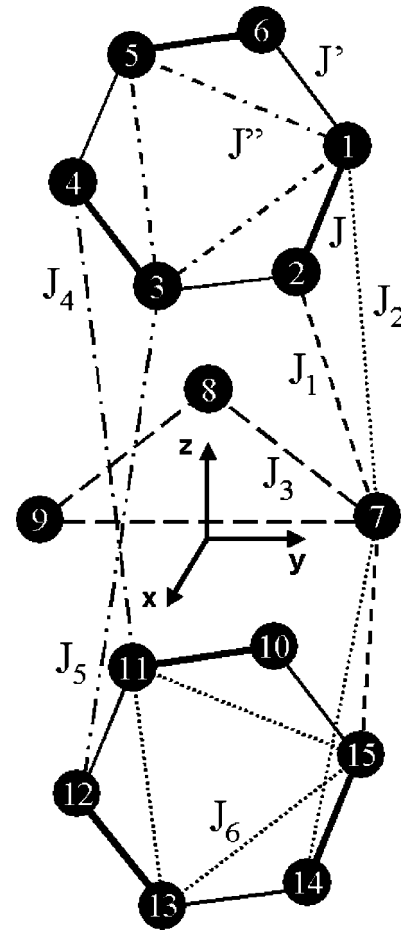

FIG. 3. Schematic diagram of the magnetic interactions in model (1) of the V$_{15}$ molecule.

tion. In this case, the gap opens symmetrically with respect to the applied field.[22] However, Ref. 22 did not address the dependence on the direction of the magnetic field. In the next section we repeat the analysis of this dependence for a 15-spin model of the V$_{15}$ molecule.

III. 15-SPIN MODEL FOR THE VANADIUM COMPLEX V$_{15}$

A. Spin interactions in V$_{15}$

In Fig. 3, we show the schematic diagram of the dominant magnetic (Heisenberg) interactions in the 15-spin model of the V$_{15}$ molecule (K$_6$[V$_{15}^{IV}$As$_6$O$_{42}$(H$_2$O)]·8H$_2$O). The magnetic structure consists of two hexagons with six $S=1/2$ spins each, enclosing a triangle with three $S=1/2$ spins. All dominant Heisenberg interactions are antiferromagnetic. The dimension of the Hilbert space of this model is $2^{15}=32\,768$. The minimal Hamiltonian is given by expression (1) with 15 instead of three spins.[22,28,29,40] The Heisenberg interactions $J_{i,j}$ in Eq. (1) between the vanadium atoms are defined according to Fig. 3. For simplicity, we assume that $\mathbf{D}_{i,j}=0$ except for bonds for which the Heisenberg exchange constant is the largest (i.e., equal to J).[29,40] Rotations of $2\pi/3$ and $4\pi/3$ around the axis perpendicular to and passing through

the center of the hexagons leave the V_{15} complex invariant. This enforces the constraints (2) and (3) on the values of $\mathbf{D}_{i,j}$.[29,30]

B. Energy-level diagrams

In this section, we will study the energy eigenvalues for various sets of parameters of the Hamiltonian, i.e., J_{ij} and/or $\mathbf{D}_{ij}$, which have so far been proposed for the 15-spin model of V_{15}.[4,18,29,40]

First let us study the case of the model parameters given in Ref. 40,

$$J = -800 \text{ K}, \quad J_1 = J' = -54.4 \text{ K},$$

$$J_2 = J'' = -160 \text{ K}, \quad J_3 = J_4 = J_5 = J_6 = 0. \quad (5)$$

In the absence of DM interactions, our method reproduces the energy gap between the ground state and the first excited state at $h=0$ to be a value of 4.124 78 K in agreement with the result of Ref. 40. This value is in reasonable agreement with the experimental value of approximately 3.7 K.[43] This energy gap causes a transition between the states $|1/2,1/2\rangle$ and $|3/2,3/2\rangle$ which takes place at $h \approx 2.8$ T (because 1 T corresponds to 1.343 K), in good agreement with the experimental value 2.8 T.

Following Ref. 30, we now take for the DM interaction parameters

$$D_{1,2}^x = D_{1,2}^y = D_{1,2}^z = 40 \text{ K}, \quad (6)$$

which is approximately 5% of the largest Heisenberg coupling. Using the rotational symmetry of the hexagon it follows from Eq. (3) that $D_{3,4}^x = 14.641$ K, $D_{3,4}^y = -54.641$ K, $D_{3,4}^z = 40$ K and $D_{5,6}^x = -54.641$ K, $D_{5,6}^y = 14.641$ K, $D_{5,6}^z = 40$ K. If the two hexagons are not equivalent we cannot reduce the number of free parameters by using a symmetry argument (see below). However, for simplicity, we may assume that the (x,y) positions of the spins on the lower hexagons differ from those on the upper hexagon by a rotation about $\pi/3$. This yields for the remaining model parameters

TABLE I. The eight lowest eigenvalues E_i and total spin S_i of the corresponding eigenstates of the V_{15} model (1) with model parameters taken from Ref. 40 for two values of the external applied field $\mathbf{h}$ parallel to the z axis. The values of the DM vectors are given in the text. The distance between E_i and the exact eigenvalue closest to E_i is $\Delta_i = \langle \varphi_i | (H - E_i)^2 | \varphi_i \rangle^{1/2} < 10^{-9}$ for $i = 1, \dots, 7$.

i	E_i ($h=0$)	S_i ($h=0$)	E_i ($h=4$ T)	S_i ($h=4$ T)
0	−3679.53623744	0.51	−3683.51181131	1.50
1	−3679.53623744	0.51	−3682.21997451	0.51
2	−3679.52777009	0.51	−3682.18488706	0.53
3	−3679.52777009	0.51	−3678.11784886	1.50
4	−3675.42943612	1.50	−3676.84225573	0.52
5	−3675.42943612	1.50	−3676.83951808	0.51
6	−3675.42325141	1.50	−3672.74011178	1.50
7	−3675.42325141	1.50	−3667.37940477	1.50

$D_{10,11}^x = -14.641$ K, $D_{10,11}^y = 54.641$ K, $D_{10,11}^z = 40$ K, $D_{12,13}^x = -40$ K, $D_{12,13}^y = -40$ K, $D_{12,13}^z = 40$ K, and $D_{14,15}^x = 54.641$ K, $D_{14,15}^y = -14.641$ K, $D_{14,15}^z = 40$ K. For this choice of model parameters, the eight lowest energies of the V_{15} model (1) for two values of the applied magnetic field ($h=0$ and $h=4$ T) along the z axis can be found in Table I. From Table I we see that for zero field the DM interaction splits the doubly degenerate doublets of $S=1/2$ states into two doublets of $S=1/2$ states. The difference in energy between the doubly degenerate, first excited states and the two fold degenerate ground states has a value of 0.0085 K. This value is much smaller than the experimental estimate of 0.05 K,[22] but of the same order of magnitude as the value cited in Ref. 29. The next four higher levels are $S=3/2$ states. The energy-level splitting between the $S=3/2$ and $S=1/2$ states is 4.1 K.

Next, we study the parameter set of Ref. 29:

$$J = -800 \text{ K}, \quad J_1 = J' = -225 \text{ K},$$

$$J_2 = J'' = -350 \text{ K}, \quad J_3 = J_4 = J_5 = J_6 = 0. \quad (7)$$

In the absence of DM interactions, the energy gap between the fourfold degenerate ground state and the first excited state is 3.61 K, in full agreement with the result of Ref. 29. Note that this value of the gap is fairly close to the experimental value of 3.7 K.[43] Taking for the DM interactions

$$D_{1,2}^x = D_{14,15}^x = 25 \text{ K},$$

$$D_{3,4}^x = D_{5,6}^x = D_{10,11}^x = D_{12,13}^x = -12.5 \text{ K},$$

$$D_{3,4}^y = -D_{5,6}^y = -D_{10,11}^y = D_{12,13}^y = -21.5 \text{ K}, \quad (8)$$

our calculation for the splitting between the two doubly degenerate $S=1/2$ levels yields 0.0037 K, about a factor of 2 larger than the value cited in Ref. 29. For the energy splitting between the $S=1/2$ and $S=3/2$ levels we obtain 3.616 K instead of the value 3.618 K given in Ref. 29. These differences seem to suggest that a perturbation approach[29] for the DM interaction may not be sufficiently accurate for quantitative purposes.[44]

Finally, we study a parameter set obtained from a first-principles calculation[18]

$$J = -809 \text{ K}, \quad J' = -120 \text{ K},$$

$$J'' = 120 \text{ K}, \quad J_1 = -30 \text{ K}, \quad J_2 = -122 \text{ K}, \quad J_3 = -3 \text{ K},$$

$$J_4 = -11 \text{ K}, \quad J_5 = -3 \text{ K}, \quad J_6 = -2 \text{ K} \quad (9)$$

(see Table I in Ref. 18). This set yields an energy gap of 4.915 K, as given in Ref. 18. Adding a DM interaction with the parameters (8) does not significantly change the energy gap between the singlet and triplet states.

In Fig. 4 we show the results for the set (7) and the DM interaction parameters of (6). For the energy gap at zero field, we find 3.7 K (instead of 4.1 K for the J's of Ref. 40), in good agreement with the experimental estimate of 3.7 K.[43]

The results for the zero-field energy gap suggest that there are many different sets of model parameters that approxi-
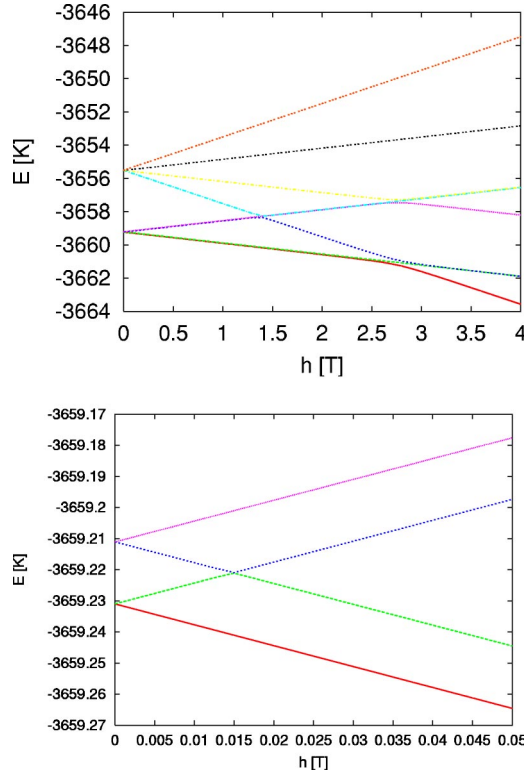
FIG. 4. (Color online) Top: The eight lowest energy levels of V_{15} model (1) with model parameters taken from Ref. 29 as a function of the applied magnetic field **h** parallel to the z axis. The values of the DM vector are given in the text. Bottom: Detailed view of the four lowest energy levels at $h \approx 0$.

mately reproduce the experimental gap between the singlet and triplet states. However, as we show below, the energy gap at zero field does not necessarily correspond to the gap of a level repulsion that is required for an adiabatic change of the magnetization.

We now study the energy-level diagram as a function of the direction of the magnetic field. As shown in the bottom panel of Fig. 4, when the field is parallel to the symmetry axis the energy levels of $M = \pm 1/2$ simply cross, just as in the case of the top panel of Fig. 1. In Fig. 5, we present results for the cases where the angle between the applied field and the z axis is 45° and 90°, respectively. Clearly, we find the same type of dependence of the energy levels on the angle of the field as in the case of the three-spin model (see bottom panel of Fig. 2 and bottom panel of Fig. 1, respectively). Exactly the same qualitative features are obtained for the other sets of parameters (7) and (9) (results not shown).

Up to now, we used DM vectors that satisfy the rotational symmetry of a hexagon, and we took the same DM vectors for the other hexagon for simplicity.[29] However, if there is some symmetry that connects the upper and lower hexagons, we have a relation between the DM vectors on both hexagons. In concert with the relations between the exchange couplings, let us assume that the upper and lower hexagons are related to each other by a 180° rotation around a vector that passes through V atom number 7 (see Fig. 3) and the middle of the line connecting the two other V atoms of the triangle. This symmetry operation X transforms the sites
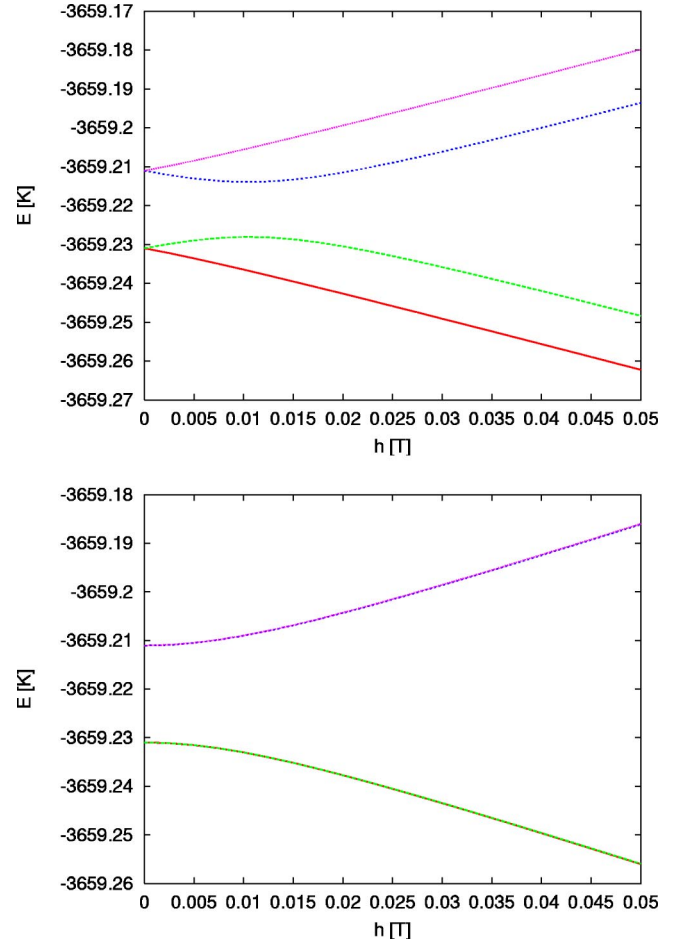

FIG. 5. (Color online) Same as the right panel in Fig. 4 except that the applied magnetic field $\mathbf{h} = h(1, 0, 1)/\sqrt{2}$ is tilted by 45° with respect to the z axis (top) and **h** is along the x axis (bottom).

$\{(1,2), (3,4), (5,6)\}$ into $\{(14,15), (10,11), (12,13)\}$. If we place the y axis along the line through V atom number 7 and through the middle of the line connecting V atoms 8 and 9, and if we take $\mathbf{D}_{1,2} = (D_x, D_y, D_z)$ as the reference DM vector, the other DM vectors are given by

$$\mathbf{D}_{3,4} = R^2 \mathbf{D}_{1,2}, \quad \mathbf{D}_{5,6} = R\mathbf{D}_{1,2},$$

$$\mathbf{D}_{14,15} = X\mathbf{D}_{1,2}, \quad \mathbf{D}_{10,11} = RX\mathbf{D}_{1,2},$$

$$\mathbf{D}_{12,13} = R^2 X\mathbf{D}_{1,2}. \tag{10}$$

Here R denotes a rotation of the hexagons around $2\pi/3$ in the plane of the hexagons. The energy-level diagrams for the set (5) and (6), with the additional constraint imposed by the above symmetry, are qualitatively similar to those obtained in Figs. 4 and 5 (results not shown).

Summarizing, as in the case of the three-spin model, all our results for the 15-spin V_{15} model clearly demonstrate that the mixing of levels strongly depends on the direction of the magnetic field. It seems therefore that this dependence is a generic feature of the DM interaction.
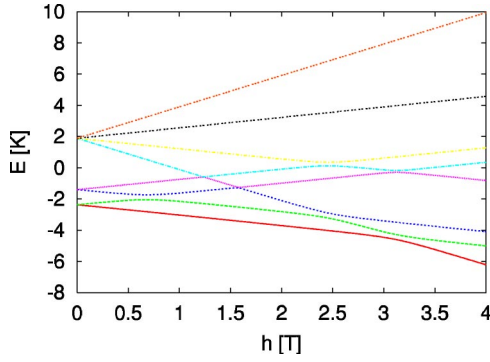
FIG. 6. (Color online) Energy-level diagram of the Hamiltonian (1) of a distorted triangle with model parameters $J_{1,2}=-2.5$ K, $J_{2,3}=-2.0$ K, $J_{3,1}=-3.0$ K, and $D_x=D_y=D_z=25$ K. The applied magnetic field $\mathbf{h}=h(1,0,1)/\sqrt{2}$ is tilted by 45° with respect to the z axis.

IV. EFFECTS OF LOWER SYMMETRY

We now discuss the effects of distortion of the triangle and anisotropic exchange interactions in the triangle model of V_{15} on the energy-level diagram for $h \approx 0$. When the triangle is distorted ($J_{1,2} \neq J_{2,3} \neq J_{3,1} \neq J_{1,2}$) the degeneracy of the two doublets at $h=0$ is lifted, even if $D_x=D_y=D_z=0$. In Figs. 6 and 7 we show data for $J_{1,2}=-2.5$ K, $J_{2,3}=-2.0$ K, and $J_{3,1}=-3.0$ K and $D_x=D_y=D_z=0.25$ K for the applied magnetic field $\mathbf{h}=h(1,0,1)/\sqrt{2}$ tilted by 45° with respect to the z axis, and for field directions parallel to the z axis and along the x axis. Unless the field is parallel to the z axis, the
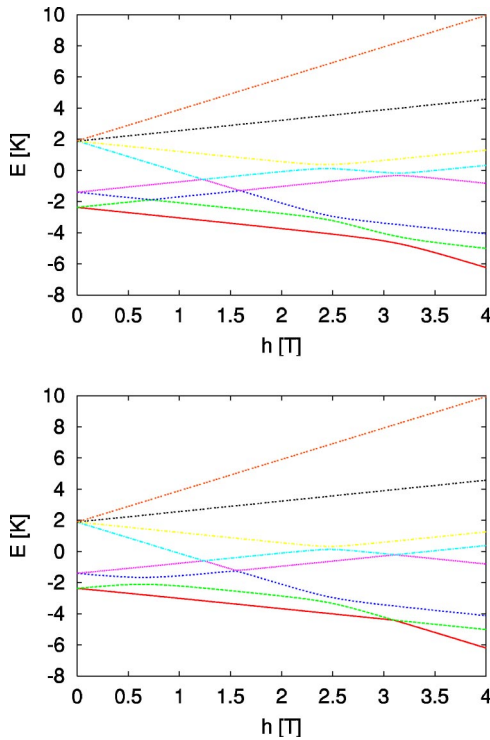

FIG. 7. (Color online) Same as Fig. 6 except that the applied magnetic field $\mathbf{h}$ is parallel to the z axis (top) and along the x axis (bottom).

energy-level diagrams are qualitatively similar to those of the undistorted triangle (see Figs. 1 and 2), that is, crossings at $h=0$ and level repulsions close to $h=0$ but not at $h=0$. However, in the case of an undistorted triangle with anisotropic, antiferromagnetic exchange interactions (i.e., different for the x,y, and z components of the spins) and $D_x=D_y=D_z=0.25$ K, the energy-level diagrams are qualitatively similar to the ones of the undistorted triangle (results not shown).

V. MANGANESE COMPLEX: Mn$_{12}$

The four inner Mn^{4+} ions in the Mn_{12} molecule $[Mn_{12}(CH_3COO)_{16}(H_2O)_4O_{12} \cdot 2CH_3COOH \cdot 4H_2O]$, have spin $S=3/2$. The other eight Mn^{3+} ions have spin $S=2$. The dimension of the Hilbert space of this system is $4^4 \times 5^8 = 10^8$. If the total magnetization is a conserved quantity, it can be used to block-diagonalize the Hamiltonian, allowing a numerical study of models of this size.[41,45] However, to study the adiabatic change of magnetization, we have to take into account all the states, and the dimension of the matrix becomes prohibitively large. Thus we need to simplify the model in order to reduce the dimension. A drastic reduction of the number of spin states can be achieved by assuming that the strong antiferromagnetic Heisenberg interaction J' between an inner ion and its outer neighbor allows the replacement of the magnetic moment of an inner ion by an effective $S=1/2$ moment. The schematic diagram of this simplified (but still complicated) model[37] is shown in the top panel of Fig. 8. The dimension of the Hilbert space of this model is $2^4 \times 5^4 = 10^4$. In the following we study this simplified model.

The Hamiltonian for the magnetic interactions of the simplified Mn_{12} model can be written as[37]

$$\mathcal{H} = -J\left(\sum_{i=1}^4 \mathbf{S}_i\right)^2 - J' \sum_{(i,j) \in \mathcal{B}} \mathbf{S}_i \cdot \mathbf{S}_j - K_z \sum_{i=1}^4 (S_{i+4}^z)^2$$

$$+ \sum_{(i,j) \in \mathcal{B}} \mathbf{D}_{i,j} \cdot [\mathbf{S}_i \times \mathbf{S}_j] - \sum_{i=1}^8 \mathbf{h} \cdot \mathbf{S}_i, \qquad (11)$$

where the index $1 \leq i \leq 4$ ($5 \leq i \leq 8$) refers to $S=1/2$ ($S=2$) spins and $\mathcal{B}$ denotes the set of pairs $\mathcal{B} = \{(1,5),(1,8),(2,5),(2,6),(3,6),(3,7),(4,6),(4,8)\}$. The first two terms describe the isotropic Heisenberg exchange between the spins. The third term (K_z) describes the single-ion easy-axis anisotropy of $S=2$ spins. The fourth term represents the antisymmetric DM interaction in Mn_{12}. The vector $\mathbf{D}_{i,j}$ determines the DM interaction between the ith $S=1/2$ spin and the jth $S=2$ spin. The last term describes the interaction of the spins with the external magnetic field $\mathbf{h}$. Note that the factor $g\mu_B$ is absorbed in our definition of $\mathbf{h}$. Model (11) reproduces experimental data, such as the splitting of the neutron scattering peaks, the results of electron paramagnetic resonance measurements, and the temperature dependence of the magnetic susceptibility.[37]

The first three terms in the Hamiltonian (11) conserve the z component of the total spin $M^z = \sum_{i=1}^8 S_i^z$. The DM interaction, on the other hand, mixes states with different total spins. Hence, the DM interaction can change level crossings
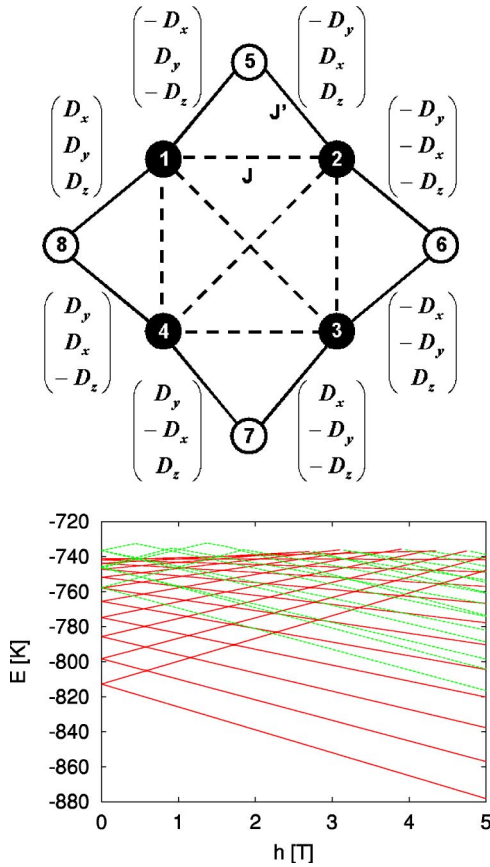
FIG. 8. Top: Schematic diagram of the magnetic interactions of the simplified model (11) of the Mn_{12} molecule (Ref. 37). Black circles, $S=1/2$; open circles, $S=2$. Also shown are the DM vectors (for $i<j$ and $\mathbf{D}_{i,j}=-\mathbf{D}_{j,i}$). Bottom: (Color online) The 21 lowest energy levels of the Mn_{12} model (11) as a function of the applied magnetic field $\mathbf{h}$. Solid lines, eigenstates with $S\approx10$; dashed lines, eigenstates with $S\approx9$. The applied magnetic field $\mathbf{h}$ is parallel to the z axis.

into level repulsions. Therefore, the presence of the DM interaction may be sufficient to explain the experimentally observed adiabatic changes of the magnetization.

The fourfold rotational-reflection symmetry (S_4) of the Mn_{12} molecule imposes some relations between the DM vectors. There are only three independent DM parameters:[37] $D_x \equiv D_{1,8}^x$, $D_y \equiv D_{1,8}^y$, and $D_z \equiv D_{1,8}^z$, as indicated in Fig. 8. The parameters of the model (11) have been estimated by comparing experimental and theoretical data. In this paper we will use the parameter set B from Refs. 37 and 42: $J=23.8$ K, $J'=79.2$ K, $K_z=5.72$ K, $D_x=22$ K, $D_y=0$, and $D_z=10$ K. Although the amount of available data is not sufficient to fix all these parameters accurately, we expect that the general trends in the energy-level diagram will not change drastically if these parameters change relatively little.

In Table II we present results for the energy and total spin of the 21 lowest states for $h=0$ and $h=5$ T (in these calculations $\mathbf{h}$ is parallel to the z axis). The numerical results obtained by full exact diagonalization (LAPACK), the Lanczos method with full orthogonalization (see Appendix B), and the Chebyshev-polynomial-based projector method (see Appendix B) are the same to working precision (about 13 dig-

its). Clearly there are states with total spin eight, nine, and ten within these 21 lowest eigenstates. Although the total magnetization is not a good quantum number, we can label the various eigenstates by their (calculated) magnetization.

The $S=10$ single-spin model for Mn_{12}

$$\mathcal{H} = -D(S^z)^2 - hS^z, \qquad (12)$$

where D denotes the uniaxial anisotropy, is often used as a starting point to interpret experimental results.[6,7,12–14,40] The energy levels of this model exhibit crossings at the resonant fields $h=\pm Dn$ for $n=-10,\ldots,10$, in qualitative agreement with our numerical results (shown in the bottom panel of Fig. 8) for the microscopic model (11). A fit of the first eight level crossings of model (12) to the data of Fig. 8 yields $D \approx 0.74$ K, in good agreement with experiments.[6,7] The Hamiltonian of the single-spin model (12) commutes with the magnetization S^z and therefore its energy diagram displays only level crossings, no level repulsions. Adding anisotropy of the form $C(S_+^4+S_-^4)$ to model (12) changes the estimated value of D and leads to level repulsions when the magnetization changes by 4.[37,46–49]

It is also of interest to compare the level splitting at $h=0$ obtained by lowest-order degenerate perturbation theory of model (12) with fourth-order anisotropy of the form $S_+^4+S_-^4$ (Refs. 47, 50, and 51)

$$\Delta E_{l+1,l} = 32D\left(\frac{C}{16D}\right)^{m/2}\frac{1}{[(m/2-1)\,!\,]^2}\frac{(S+m)!}{(S-m)!}, \quad (13)$$

for m even ($\Delta E_{l+1,l}=0$ for m odd) with the result of the microscopic model calculation based on model (11). In Eq. (13) l denotes the perturbed eigenstates in increasing order of energy and m is the magnetic quantum number of the unperturbed states.[47] Using the values $D\approx0.69$ K, $C/D\approx5.7\times10^{-5}$ obtained by fitting the single-spin model to experimental data,[47] the energy gap for $m=6$ is given by

$$\Delta E_{13,12} \approx 0.000\,22\ \mathrm{K}. \qquad (14)$$

Taking into account that (because of the presence of $S\approx9$ states) the corresponding $S\approx10$ levels of model (11) are the 14th and 15th lowest energy levels, Table II shows that for $h=0$, $\Delta E_{13,12}=0.000\,42$ K. In view of the uncertainties on the estimates of the various model parameters, the difference of only a factor of 2 is remarkably small. From this comparison, we may conclude that the DM interaction leads to energy gaps that are of the same order of magnitude as the gaps due to the fourth-order terms $S_+^4+S_-^4$ in the single-spin model.

In the bottom panel of Fig. 8 we show the results for the lowest 21 energy levels of the Mn_{12} model as a function of the applied magnetic field as obtained by LFO. The applied magnetic field is parallel to the z axis. In Fig. 8 solid (dashed) lines represent eigenstates with $S\approx10$ (9) (within an error of about 10%). Also eigenstates with $S\approx8$ appear for $h>4$ but these are not shown for clarity. For the Mn_{12} model, the DM induced energy splittings between the $S\approx10,M\approx-10$ state and other states are less than 10^{-6} K. Adding an extra transverse field by tilting the $\mathbf{h}$ field by 5° with respect to the z axis does not change this conclusion (results not shown).

TABLE II. The 21 lowest eigenvalues E_i and total spin S_i of the corresponding eigenstates of the Mn_{12} model (11) for two values of the external applied field **h** along the z axis. The distance between E_i and the exact eigenvalue closest to E_i is $\Delta_i = \langle \varphi_i | (H - E_i)^2 | \varphi_i \rangle^{1/2} < 10^{-10}$ for $i = 1, \dots, 7$. Note that for $h = 0$ the levels 12, 13, 18, 19, and 20 belong to the $S \approx 9$ subspace and not to the $S \approx 10$ subspace.

i	$E_i \, (h=0)$	$S_i \, (h=0)$	$E_i \, (h=5 \text{ T})$	$S_i \, (h=5 \text{ T})$
0	−812.771882673675	9.72	−878.203468556749	9.77
1	−812.771882673460	9.72	−857.042137859145	9.78
2	−798.326618260922	9.72	−837.727273846391	9.76
3	−798.326618261122	9.72	−820.218084451590	9.73
4	−785.677644659194	9.70	−816.530388063144	8.82
5	−785.677644658983	9.70	−804.449056631056	9.69
6	−774.774953284432	9.68	−804.242954124067	8.77
7	−774.774953284294	9.68	−798.519706376890	8.82
8	−765.549187817101	9.65	−790.336285910398	9.65
9	−765.549187333902	9.65	−788.717912654407	8.78
10	−757.919915510036	9.61	−782.037906282298	8.82
11	−757.919915509970	9.61	−777.789121186874	9.60
12	−757.673722613912	8.77	−774.222534072884	8.79
13	−757.673722613981	8.77	−773.614730624955	8.80
14	−751.806498916496	9.57	−766.993852023410	8.80
15	−751.806072514140	9.57	−766.720405060281	9.55
16	−747.135398548595	9.54	−760.807893152451	8.79
17	−747.135398548602	9.54	−760.482768227423	8.12
18	−746.357522623039	8.77	−757.060762637193	9.51
19	−746.357522623082	8.77	−754.700878489864	8.59
20	−745.778951523327	8.70	−753.310517350023	8.78

Finally, we added to model (11) the next-to-lowest order relativistic correction to the local anisotropy that is compatible with the symmetry of the square[37]

$$\mathcal{H}_1 = K_1[(S_1^x)^2 + (S_2^y)^2 + (S_3^x)^2 + (S_4^y)^2]. \qquad (15)$$

Although we took a perhaps unrealistically large value of K_1 ($K_1 = K_z/2$), we were unable to detect energy-level repulsions up to the $M \approx -10, M \approx 3$ transition (results not shown). On the other hand, in experiments,[6,7,12] adiabatic changes of the magnetization have been observed at $h \approx 3.4$ T ($M_z \approx -10 \rightarrow M_z \approx 4$) and $h \approx 3.9$ T ($M_z \approx -10 \rightarrow M_z \approx 3$) and the magnitude of the energy splittings is of the order of 10 nK.[43] The precision of the present calculations is about 10^{-6} K. Thus, it is consistent that within the (very high) resolution in the **h** field and the 13-digit precision of the calculation, no information about the gap could be extracted. The algorithms developed for the work presented in this paper can be used for 33-digit calculations without modification.

It has already been demonstrated that the many-spin model (11) can reproduce neutron scattering data, high-frequency electron spin resonance, and the temperature dependence of the magnetic susceptibility of the Mn_{12} system.[37] Our results for the energy-level diagram show features (for example, the presence of $S=9$ levels, see Fig. 8) that are not accounted for by a single-spin $S=10$ model for

Mn_{12}. In Sec. III we discussed the properties of the level repulsions due to the DM interactions in the V_{15} system. For the Mn_{12} system we expect to find similar behavior. However, we find that the energy differences at the crossing points are smaller than the 10^{-6} K accuracy of our numerical calculations. Therefore in this section we studied the main features of the energy-level diagram of Mn_{12}. In principle, it is possible to leave the $S \approx 10$ multiplet by sweeping the magnetic field but for Mn_{12} the probabilities for these transitions are also smaller than the 10^{-6} K accuracy of our numerical calculations. Finally, there is the possibility that couplings such as the hyperfine interaction also yield level repulsions with energy-level splittings that are significantly larger than those generated by the DM interaction. We leave the study of these interesting topics for future research.

VI. DISCUSSION

We have studied the dependence of the energy-level diagrams, with level repulsions due to the Dzyaloshinskii-Moriya interaction, on the direction of the applied magnetic field. We found that the dependence on the direction of the magnetic field seems to be generic, at least if the system has C_3 symmetry. Our numerical data suggest that the three-spin model reproduces the main features of the 15-spin model of V_{15}. The presence of the Dzyaloshinskii-Moriya interaction allows for adiabatic changes of the magnetization but, ac-

cording to our calculations, the value of the resonant field for the $|1/2,-1/2\rangle$ to $|1/2,1/2\rangle$ transition changes with the direction of the magnetic field. The Dzyaloshinskii-Moriya interaction not only lifts the degeneracy but, depending on the direction of the field with respect to the symmetry axis, also shifts the resonant point away from $h=0$.

The butterfly hysteresis loop observed in time-resolved magnetization measurements has been interpreted in terms of a combination of a Landau-Zener-Stückelberg transition at zero field and spin-phonon coupling.[16,22] Our results show that unless the field is applied in a special direction (x or y direction in this case), the adiabatic magnetization process is no longer symmetric with respect to the field. The dependence on the direction of the field should lead to observable changes in the hysteresis loops. So far, only weak directional dependence has been reported in experiments.[43] Therefore, it seems that it is necessary to explore other mechanisms that yield energy-level repulsions such as hyperfine interactions.[52]

APPENDIX A: DIAGONALIZATION OF MODEL (1)

Here we collect some analytical results of the solution of the eigenvalue problem of Hamiltonian (1). We consider only the case of a magnetic field that is parallel to the z axis [$\mathbf{h}=(0,0,h_z)$]. For a DM vector satisfying the conditions (2) and (3) the eight eigenvalues are given by

$$E_{0,1} = \frac{-\sqrt{3}D_z + 4h_z \pm \sqrt{9D_x{}^2 + 9D_y{}^2 + (\sqrt{3}D_z - 3J + 2h_z)^2}}{4},$$

$$E_{2,3} = \frac{-\sqrt{3}D_z - 4h_z \pm \sqrt{9D_x{}^2 + 9D_y{}^2 + (\sqrt{3}D_z - 3J - 2h_z)^2}}{4},$$

$$E_{4,5} = \frac{\sqrt{3}D_z \pm \sqrt{3D_x{}^2 + 3D_y{}^2 + (\sqrt{3}D_z + 3J - 2h_z)^2}}{4},$$

$$E_{6,7} = \frac{\sqrt{3}D_z \pm \sqrt{3D_x{}^2 + 3D_y{}^2 + (\sqrt{3}D_z + 3J + 2h_z)^2}}{4},$$

$$(A1)$$

where $D_x = D_{1,2}^x$, $D_y = D_{1,2}^y$, and $D_z = D_{1,2}^z$. Substituting the values of all model parameters, we recover the results obtained by numerical diagonalization. For $h_z = 0$ there are four pairs of twofold degenerate levels. Although it is possible to find analytical expressions for the case that the magnetic

field is parallel to the x axis, the expressions themselves are rather long and not very illuminating. Therefore they are not given here.

For a magnetic field parallel to the z axis, a straightforward calculation shows that

$$\mathcal{H}|3/2,3/2\rangle = -\frac{3(J + 2h_z)}{4}|3/2,3/2\rangle + \frac{3(D_x + iD_y)}{4}|a\rangle,$$

$$\mathcal{H}^2|3/2,3/2\rangle = \frac{9[(J+2h_z)^2 + D_x^2 + D_y^2]}{16}|3/2,3/2\rangle$$
$$-\frac{3(D_x + iD_y)(\sqrt{3}D_z + 4h_z)}{8}|a\rangle,$$

$$\mathcal{H}|3/2,1/2\rangle = -\frac{3J + 2h_z}{4}|3/2,1/2\rangle - \frac{\sqrt{3}(D_x + iD_y)}{4}|\bar{a}\rangle,$$

$$\mathcal{H}^2|3/2,1/2\rangle = \frac{(3J + 2h_z)^2 + 3(D_x^2 + D_y^2)}{16}|3/2,1/2\rangle$$
$$-\frac{3(D_x + iD_y)D_z}{8}|\bar{a}\rangle, \qquad (A2)$$

where $|\bar{a}\rangle$ denotes the state $|a\rangle$ with all spins reversed and

$$|a\rangle = \frac{1}{2\sqrt{3}}\big[(1 - i\sqrt{3})|\downarrow\uparrow\uparrow\rangle$$
$$+ (1 + i\sqrt{3})|\uparrow\downarrow\uparrow\rangle - 2|\uparrow\uparrow\downarrow\rangle\big]. \qquad (A3)$$

The expressions for $\mathcal{H}|3/2,-3/2\rangle$, $\mathcal{H}^2|3/2,-3/2\rangle$, $\mathcal{H}|3/2,-1/2\rangle$, and $\mathcal{H}^2|3/2,-1/2\rangle$ are obtained from Eqs. (A2) and (A3) by changing the sign of h_z and D_y and replacing $|a\rangle$ by

$$|b\rangle = \frac{-1}{2\sqrt{3}}\big[(1 - i\sqrt{3})|\uparrow\downarrow\downarrow\rangle$$
$$+ (1 + i\sqrt{3})|\downarrow\uparrow\downarrow\rangle - 2|\downarrow\downarrow\uparrow\rangle\big]. \qquad (A4)$$

Note that $\langle a|b\rangle = 0$. From Eq. (A2) it follows that for the external field parallel to the z axis, model (1) does not allow transitions from the state with all spins up (down) to the state with two spins down (up). Therefore, if initially the system is in the state with all spins down, adiabatically sweeping the field from a large negative value to a large positive value will *not* yield the final state with all spins up.

APPENDIX B: NUMERICAL METHODS

A theoretical description of quantum dynamical phenomena in the Mn_{12} and V_{15} nanomagnets requires detailed knowledge of their energy-level schemes. Disregarding the fascinating physics of the nanomagnets, the calculation of the eigenvalues of their model Hamiltonians is a challenging problem in its own right. First, the (adiabatic) quantum dynamics of these systems is mainly determined by the (tiny) level repulsions. Therefore the calculation of the energy levels of these many-spin Hamiltonians has to be very accurate in order to bridge the energy scales involved (e.g., from

500 K to $\approx 10^{-19}$ K). Second, the level repulsions originate from the DM interactions which mix states with different magnetization. In principle, this prevents the use of the magnetization as a vehicle to block-diagonalize the Hamiltonian and effectively reduce the size of the matrices that have to be diagonalized. If a level repulsion involves states of significantly different magnetization (e.g., $M^z = -10$ and $M^z = 10$) a perturbative calculation of the level splitting would require going to rather high order (at least 20), a cumbersome procedure. Therefore it is of interest to explore alternative routes to direct but accurate, brute-force diagonalization of the full model Hamiltonian.

As a nontrivial set of reference data, we used the eigenvalues obtained by full diagonalization (using standard LAPACK algorithms) of the $10\,000 \times 10\,000$ matrix representing model (11).[42] For one set of model parameters, such a calculation takes about 2 h of CPU time on an Athlon 1.8 GHz, 1.5 Gbytes system. Clearly this is too slow if we want to compute the energy-level diagram, in particular if we want to estimate the structure of the level splittings. At the resonant fields we need the eigenvalues for many values of **h**. Furthermore, in the case of V_{15} this calculation would take about 30 times longer and require about 15 Gbytes of memory which, for present-day computers, is too much to be of practical use.

We have tested different standard algorithms to compute the low-lying eigenvalues of large matrices. The standard Lanczos method (including its conjugate gradient version) as well as the power method[53,54] either converge too slowly, lack the accuracy to resolve the (nearly) degenerate eigenvalues, on sometimes even completely fail to correctly reproduce the low-lying part of the spectrum. This is not a surprise. By construction these methods work well if the ground state is not degenerate and there is little guarantee that they will work if there are (nearly) degenerate eigenvalues.[53,54] In particular, the Lanczos procedure suffers from numerical instabilities due to the loss of orthogonalization of the Lanczos vectors.[53,54] It seems that model Hamiltonians for the nanoscale magnets provide a class of (complex Hermitian) eigenvalue problems that are hard to solve.

Extensive tests led us to the conclusion that only the Lanczos method with full orthogonalization[53,54] and the Chebyshev-polynomial-based projector method discussed below can solve these rather large and difficult eigenvalue problems with sufficient accuracy. The former is significantly faster than the latter but using both gives extra confidence in the results.

1. Lanczos method with full orthogonalization

In the LFO, each time a new Lanczos vector is generated we explicitly orthogonalize (to working precision) this vector to all, not just to the two previous, Lanczos vectors.[53,54] With some minor modifications to restart the procedure when the Lanczos iteration terminates prematurely, after n steps this procedure transforms the $n \times n$ matrix H into a tridiagonal matrix that is comparable in accuracy to the one obtained through Householder tridiagonalization but offers no advantages.[54] In our case we are interested only in a few

low-lying eigenstates of H. Thus we can exploit the fact that projection onto the (numerically exact) subspace of dimension k ($k \ll n$) built by the Lanczos vectors will yield increasingly accurate estimates of the smallest (largest) eigenvalues and corresponding eigenvectors as k increases.

In practice, to compute the M lowest energy levels, the LFO procedure is carried out as follows.

(1) Perform a Lanczos step according to the standard procedure.

(2) Use the modified Gramm-Schmidt procedure to orthogonalize the new Lanczos vector with respect to all previous ones.[53,54]

(3) Compute the matrix elements of the tridiagonal matrix.

(4) At regular intervals, diagonalize the tridiagonal matrix, compute the approximate eigenvectors φ_i, $\mu_i = \langle \varphi_i | H | \varphi_i \rangle$, and $\Delta_i^2 = \langle \varphi_i | (H - \mu_i)^2 | \varphi_i \rangle$ for $i = 1, \ldots, M$, and check if all Δ_i are smaller than a specified threshold. If so, terminate the procedure (the exact eigenvalue E_i closest to μ_i satisfies $\mu_i - \Delta \leq E_i \leq \mu_i + \Delta_i$). If not, continue generating new Lanczos vectors, etc.

2. Chebyshev polynomial projector method

As an alternative to the LFO, we have used a power method[53,54] based on the matrix exponential e^{-tH}.[55] Writing the random vector $\Psi(0)$ in terms of the (unknown) eigenvectors $\{\phi_i\}$ of H, we find

$$\Psi(t) = e^{-tE_0}[\phi_0 \langle \phi_0 | \Psi(0) \rangle + e^{-t(E_1 - E_0)} \phi_1 \langle \phi_1 | \Psi(0) \rangle$$
$$+ e^{-t(E_2 - E_0)} \phi_2 \langle \phi_2 | \Psi(0) \rangle + \cdots], \quad \text{(B1)}$$

showing $\lim_{t \to \infty} \Psi(t)/\|\Psi(t)\| \propto \phi_0$ if $\langle \phi_0 | \Psi(0) \rangle \neq 0$. In this naive matrix-exponential version of the power method, convergence to the lowest eigenstate is exponential in t if $E_1 > E_0$.

The case of degenerate ($E_0 = E_1 = \cdots$) or very close ($E_0 \approx E_1 \approx \cdots$) eigenvalues can be solved rather easily by applying the projector to a subspace instead of a single vector, in combination with diagonalization of e^{tH} within this subspace.[55] First we fix the dimension k of the subspace by taking k equal to or larger than the desired number of distinct eigenvalues. The projection parameter t should be as large as possible but nevertheless sufficiently small so that at least the first k terms survive one projection step. Then we generate a set of random initial vectors $\Psi_i(0)$ for $i = 1, \ldots, k$ and set the projection count n to zero. We compute the k lowest eigenstates by the following algorithm.[55]

(1) Perform a projection step $\Psi_i[(n+1)t] = e^{-tH}\Psi_i(nt)$ for $i = 1, \ldots, k$.

(2) Compute the $k \times k$ matrices. $A = \langle \Psi_i[(n+1)t] | e^{tH} | \Psi_i[(n+1)t] \rangle = \langle \Psi_i[(n+1)t] | \Psi_i(nt) \rangle$ and $B = \langle \Psi_i[(n+1)t] | \Psi_i[(n+1)t] \rangle$. Note that A is Hermitian and B is positive definite.

(3) Determine the unitary transformation U that solves the $k \times k$ generalized eigenvalue problem $Ax = \lambda Bx$. Recall that k is small.

(4) Compute $\Psi_i'[(n+1)t] = \sum_{j=1}^{k} U_{i,j} \Psi_j[(n+1)t]$ for $i = 1, \ldots, k$.

(5) Set $\Psi_i[(n+1)t] = \Psi_i'[(n+1)t]$ for $i = 1, \ldots, k$.

(6) Compute $\mu_i = \langle \Psi_i[(n+1)t] | H | \Psi_i[(n+1)t] \rangle$ and check if $\Delta_i^2 = \langle \Psi_i[(n+1)t] | (H - \mu_i)^2 | \Psi_i[(n+1)t] \rangle$ is smaller than a specified threshold for $i = 1, \ldots, k$. If yes, terminate the calculation. If no, increase n by 1 and repeat the procedure.

We calculate $e^{-tH}\Psi$ by using the Chebyshev polynomial expansion method.[56–60] First we compute an upper bound R of the spectral radius of H (i.e., $\|H\| \leq R$) by repeatedly using the triangle inequality.[60] From this point on we use the "normalized" matrix $\tilde{H} = (2H/R - 1)/2$. The eigenvalues of the Hermitian matrix $\tilde{H}$ are real and lie in the interval $[-1, 1]$.[53,54] Expanding the initial value $\Psi(0)$ in the (unknown) eigenvectors ϕ_j of $\tilde{H}$ (or H) we find

$$\Psi(t) = e^{-tH}\Psi(0) = e^{z\tilde{H}}\Psi(0) = \sum_j e^{z\tilde{E}_j} \phi_j \langle \phi_j | \Psi(0) \rangle,$$

(B2)

where $z = -tR$. We find the Chebyshev polynomial expansion of $\Psi(t)$ by computing the Fourier coefficients of the function $e^{z\cos\theta}$.[61] Alternatively, since $-1 \leq \tilde{E}_j \leq 1$, we can use the expansion $e^{z\tilde{E}_j} = I_0(z) + 2\sum_{m=1}^{\infty} I_m(z) T_m(\tilde{E}_j)$ where $I_m(z)$ is the modified Bessel function of integer order m (Ref. 61) to write Eq. (B2) as

$$\Psi(t) = \left[I_0(z)I + 2\sum_{m=1}^{\infty} I_m(z) T_m(\tilde{H}) \right] \Psi(0). \qquad \text{(B3)}$$

Here, I is the identity matrix and $T_m(\tilde{H})$ is the matrix-valued Chebyshev polynomial defined by the recursion relations

$$T_0(\tilde{H})\Psi(0) = \Psi(0), \quad T_1(\tilde{H})\Psi(0) = \tilde{H}\Psi(0), \qquad \text{(B4)}$$

and

$$T_{m+1}(\tilde{H})\Psi(0) = 2\tilde{H}T_m(\tilde{H})\Psi(0) - T_{m-1}(\tilde{H})\Psi(0), \qquad \text{(B5)}$$

for $m \geq 1$. In practice we will sum only contributions with $m \leq M$ where M is chosen such that, for all $m > M$, $|I_m(z)/I_0(z)|$ is zero to machine precision. Then it is not difficult to show that $\|e^{-tH}/I_0(z) - I - 2\sum_{m=1}^{M}[I_m(z)/I_0(z)]T_m(\tilde{H})\|$ is zero to machine precision too [instead of e^{-tH} we can equally well use $e^{-tH}/I_0(z)$ as the projector].

Using the downward recursion relation of the modified Bessel functions, we can compute K Bessel functions to machine precision using of the order of K arithmetic operations.[61,62] A calculation of the first 20 000 modified Bessel functions takes less than 1 s on a Pentium III 600 MHz mobile processor, using 14–15 digit arithmetic. Hence this part of a calculation is a negligible fraction of the total computational work for solving the eigenvalue problem. Performing one projection step with e^{-tH} amounts to repeatedly using recursion (B5) to obtain $\tilde{T}_m(B)\Psi(0)$ for $k = 2, \ldots, M$, multiply the elements of this vector by $I_m(z)$, and add all contributions.

---

*Electronic address: deraedt@phys.rug.nl; URL: http://www.compphys.org

†Electronic address: miya@spin.t.u-tokyo.ac.jp

‡Electronic address: kristel@phys.rug.nl

§Electronic address: machida@spin.t.u-tokyo.ac.jp

[1] *Quantum Tunneling of Magnetization*, Vol. 301 of NATO Advanced Study Institute, Series E: Applied Sciences, edited by L. Gunther and B. Barbara (Kluwer, Dordrecht, 1995).

[2] A. Caneschi, D. Gatteschi, R. Sessoli, A. Barra, L. C. Brunel, and M. Guillot, J. Am. Chem. Soc. **113**, 5873 (1991).

[3] R. Sessoli, H.-L. Tsai, A. R. Shake, S. Wang, J. B. Vincent, K. Folting, D. Gatteschi, G. Christou, and D. N. Hendrickson, J. Am. Chem. Soc. **115**, 1804 (1993).

[4] D. Gatteschi, L. Pardi, A. L. Barra, and A. Müller, Mol. Eng. **3**, 157 (1991).

[5] G. Levine and J. Howard, Phys. Rev. Lett. **75**, 4142 (1995).

[6] J. R. Friedman, M. P. Sarachik, J. Tejada, and R. Ziolo, Phys. Rev. Lett. **76**, 3830 (1996).

[7] L. Thomas, F. Lionti, R. Ballou, D. Gattesehi, R. Sessoli, and B. Barbara, Nature (London) **383**, 145 (1996).

[8] C. Sangregorio, T. Ohm, C. Paulsen, R. Sessoli, and D. Gatteschi, Phys. Rev. Lett. **78**, 4645 (1997).

[9] W. Wernsdorfer and R. Sessoli, Science **284**, 133 (1999).

[10] W. Wernsdorfer, T. Ohm, C. Sangregorio, R. Sessoli, D. Mailly, and C. Paulsen, Phys. Rev. Lett. **82**, 3903 (1999).

[11] B. Barbara, L. Thomas, F. Lionti, A. Sulpice, and A. Caneschi, J. Magn. Magn. Mater. **177**, 1324 (1998).

[12] J. A. A. J. Perenboom, J. S. Brooks, S. Hill, T. Hathaway, and N. S. Dalal, Phys. Rev. B **58**, 330 (1998).

[13] I. Chiorescu, W. Wernsdorfer, A. Müller, H. Bögge, and B. Barbara, Phys. Rev. Lett. **84**, 3454 (2000).

[14] T. Pohjola and H. Schoeller, Phys. Rev. B **62**, 15 026 (2000).

[15] Y. Zhong, M. P. Sarachik, J. Yoo, and D. N. Hendrickson, Phys. Rev. B **62**, R9256 (2000).

[16] I. Chiorescu, W. Wernsdorfer, A. Müller, H. Bögge, and B. Barbara, J. Magn. Magn. Mater. **221**, 103 (2000).

[17] I. Chiorescu, R. Giraud, A. G. M. Jansen, A. Caneschi, and B. Barbara, Phys. Rev. Lett. **85**, 4807 (2000).

[18] D. W. Boukhvalov, V. V. Dobrovitski, M. I. Katsnelson, A. I. Lichtenstein, B. N. Harmon, and P. Kögerler, J. Appl. Phys. **93**, 7082 (2003).

[19] D. W. Boukhvalov, A. I. Lichtenstein, V. V. Dobrovitski, M. I. Katsnelson, B. N. Harmon, V. V. Mazurenko, and V. I. Anisimov, Phys. Rev. B **65**, 184435 (2002).

[20] W. Wernsdorfer, N. Allaga-Alcalde, D. N. Hendrickson, and G. Christou, Nature (London) **416**, 407 (2002).

[21] A. Honecker, F. Meier, D. Loss, and B. Normand, Eur. Phys. J. B **27**, 487 (2002).

[22] I. Chiorescu, W. Wernsdorfer, A. Müller, S. Miyashita, and B. Barbara, Phys. Rev. B **67**, 020402 (2003).

[23] S. Miyashita, J. Phys. Soc. Jpn. **64**, 3207 (1995).

[24] S. Miyashita, J. Phys. Soc. Jpn. **65**, 2734 (1996).

[25] V. V. Dobrovitskii and A. K. Zvezdin, Europhys. Lett. **38**, 377 (1997).

[26] L. Gunther, Europhys. Lett. **39**, 1 (1997).

[27] H. De Raedt, S. Miyashita, K. Saitoh, D. García-Pablos, and N. García, Phys. Rev. B **56**, 11 761 (1997).

[28] S. Miyashita and N. Nagaosa, Prog. Theor. Phys. **106**, 533 (2001).

[29] N. P. Konstantinidis and D. Coffey, Phys. Rev. B **66**, 174426 (2002).

[30] I. Rudra, K. Saitoh, S. Ramasesha, and S. Miyashita, cond-mat/0212354 (unpublished).

[31] T. A. Kaplan, Z. Phys. B: Condens. Matter **49**, 313 (1983).

[32] L. Shekhtman, O. Entin-Wohlman, and A. Aharony, Phys. Rev. Lett. **69**, 836 (1992).

[33] L. Shekhtman, A. Aharony, and O. Entin-Wohlman, Phys. Rev. B **47**, 174 (1993).

[34] A. Zheludev, S. Maslov, I. Tsukada, I. Zaliznyak, L. P. Regnault, T. Masuda, K. Uchinokura, R. Erwin, and G. Shirane, Phys. Rev. Lett. **81**, 5410 (1998).

[35] I. E. Dzyaloshinskii, Zh. Eksp. Teor. Fiz. **32**, 1547 (1957) [Sov. Phys. JETP **5**, 1259 (1957)].

[36] T. Moriya, Phys. Rev. **120**, 91 (1960).

[37] M. I. Katsnelson, V. V. Dobrovitski, and B. N. Harmon, Phys. Rev. B **59**, 6919 (1999).

[38] M. Al-Saqer, V. V. Dobrovitski, B. N. Harmon, and M. I. Katsnelson, J. Appl. Phys. **87**, 6268 (2000).

[39] I. Rudra, S. Ramasesha, and D. Sen, Phys. Rev. B **64**, 014408 (2001).

[40] I. Rudra, S. Ramasesha, and D. Sen, J. Phys.: Condens. Matter **13**, 11717 (2001).

[41] C. Raghu, I. Rudra, D. Sen, and S. Ramasesha, Phys. Rev. B **64**, 064419 (2001).

[42] H. De Raedt, A. H. Hams, V. V. Dobrovitsky, M. Al-Saqer, M. I. Katsnelson, and B. N. Harmon, J. Magn. Magn. Mater. **246**, 392 (2002).

[43] I. Chiorescu (private communication).

[44] V. V. Kostyuchenko and A. K. Zvezdin, Phys. Solid State **45**, 903 (2003).

[45] N. Regnault, Th. Jolicoeur, R. Sessoli, D. Gatteschi, and M. Verdaguer, Phys. Rev. B **66**, 054409 (2002).

[46] A. L. Barra, D. Gatteschi, and R. Sessoli, Phys. Rev. B **56**, 8192 (1997).

[47] F. Luis, F. Bartolomé, and J. Fernández, Phys. Rev. B **57**, 505 (1998).

[48] S. Hill, J. A. A. J. Perenboom, N. S. Dalal, T. Harthaway, T. Stalcup, and J. S. Brooks, Phys. Rev. Lett. **80**, 2453 (1998).

[49] E. Del Barco, A. D. Kent, E. M. Rumberger, D. N. Hendrickson, and G. Christou, Europhys. Lett. **60**, 768 (2002).

[50] D. A. Garanin, J. Phys. A **24**, L61 (1991).

[51] D. A. Garanin and E. M. Chudnovsky, Phys. Rev. B **59**, 3671 (1997).

[52] S. Miyashita, H. De Raedt, and K. Michielsen, Prog. Theor. Phys. **110**, 889 (2003).

[53] J. H. Wilkinson, *The Algebraic Eigenvalue Problem* (Clarendon Press, Oxford, 1965).

[54] G. H. Golub and C. F. Van Loan, *Matrix Computations* (Johns Hopkins University Press, Baltimore, 1996).

[55] H. De Raedt, Comput. Phys. Rep. **7**, 1 (1987).

[56] H. Tal-Ezer and R. Kosloff, J. Chem. Phys. **81**, 3967 (1984).

[57] T. Iitaka, S. Nomura, H. Hirayama, X. Zhao, Y. Aoyagi, and T. Sugano, Phys. Rev. E **56**, 1222 (1997).

[58] C. Leforestier, R. H. Bisseling, C. Cerjan, M. D. Feit, R. Friesner, A. Guldberg, A. Hammerich, G. Jolicard, W. Karrlein, H.-D. Meyer, N. Lipkin, O. Roncero, and R. Kosloff, J. Comput. Phys. **94**, 59 (1991).

[59] R. N. Silver and H. Röder, Phys. Rev. E **56**, 4822 (1997).

[60] V. V. Dobrovitski and H. A. De Raedt, Phys. Rev. E **67**, 056702 (2003).

[61] *Handbook of Mathematical Functions*, edited by M. Abramowitz and I. Stegun (Dover, New York, 1964).

[62] W. H. Press, B. P. Flannery, S. A. Teukolsky, and W. T. Vetterling, *Numerical Recipes* (Cambridge University Press, New York, 1986).